RMetS
Royal Meteorological Society

# On steady-state tropical cyclones

Roger K. Smith,[a]* Michael T. Montgomery[b] and John Persing[b]
[a]*Meteorological Institute, Ludwig Maximilians University of Munich, Germany*
[b]*Department of Meteorology, Naval Postgraduate School, Monterey, CA, USA*

*Correspondence to: R. K. Smith, Meteorological Institute, Ludwig Maximilians University of Munich, Theresienstr. 37, 80333 Munich, Germany. E-mail: roger.smith@lmu.de



**We examine the physical constraints that must be satisfied to allow for a steady-state tropical cyclone in an isolated environment, paying particular attention to the need to replenish absolute angular momentum at exactly the rate at which it is consumed and to the vanishing of the spin-up function above the frictional boundary layer. We conclude that it is unlikely that these conditions will be met simultaneously and question whether globally steady-state tropical cyclone solutions have merit. The implications for previous studies are discussed.**

*Key Words:* hurricanes; tropical cyclones; typhoons; steady-state

*Received 18 April 2013; Revised 25 November 2013; Accepted 29 December 2013; Published online in Wiley Online Library 30 May 2014*

## 1. Introduction

This study is motivated by several questions that have arisen in our own work and that of several others surrounding the concept of the 'mature stage' of a hurricane vortex. The definition of the 'mature stage' is commonly based on the time period in which the maximum tangential wind speed is approximately constant. However, in many of our own calculations the upper and outer circulations are by no means steady at this stage. In some cases the storm continues to expand in size in the lower troposphere, while in other cases it has already begun to contract. In the few extended-range calculations that we have carried out, the vortex intensity decreases with time after some period of maximum intensity, although the upper anticyclone may continue to intensify after the inner vortex core has begun to decay. To focus on these issues, we consider the possibility of a global steady-state solution for the idealized problem of an isolated tropical cyclone vortex on an $f$-plane. By steady state, we mean that the macro-scale flow does not vary systematically with time.

A globally steady state would require first that the convective instability in the core region of the storm be maintained by fluxes of moisture at the underlying sea surface and/or radiative cooling of the upper atmosphere. The convective heating in the inner-core region and the radiative cooling provide a pattern of net diabatic heating that forces an overturning, in-up-and-out, circulation (Ooyama, 1969; Shapiro and Willoughby, 1982). Above the frictional boundary layer, this steady-state circulation must be along absolute angular momentum (or $M$-) surfaces (see section 2). In the upward branch of the secondary circulation, the diabatic heating rate associated with moist convection must be consistent with the approximate material conservation of pseudo-equivalent potential temperature, $\theta_e$. In the descending branch of the circulation, where radiative cooling is mainly operative, $\theta_e$ is not materially conserved. However, the radiative cooling must exactly balance the adiabatic warming of air parcels as they descend. Above the boundary layer, these conditions are encapsulated by the need for the spin-up function, $S$, to vanish, as discussed in section 3.2.

The severity of the global constraint associated with $S \equiv 0$ alone led Smith *et al.* (2013) and Persing *et al.* (2013) to question the theoretical existence of a globally steady tropical cyclone within the framework of balance dynamics. However, there are other issues, since the foregoing simple picture assumes that the upward branch of the secondary circulation takes place in the eyewall and that elsewhere there is subsidence. This subsidence would bring extremely dry air from the upper troposphere to the surface. Another layer of complexity is the existence of rain bands, shallow convection and convection of moderate vertical extent that serve to moisten the dry air descending into the boundary layer. In addition, a global steady state would require just the fluxes of sensible and latent heat necessary to maintain the foregoing thermodynamic cycle.

Fourty years ago, Anthes (1974) pointed out that, for a tropical cyclone to achieve a steady state, there would have to be an input of *cyclonic relative* angular momentum to replenish that lost by friction to the sea surface. As shown herein, this input requires either a radial cyclonic eddy angular momentum flux at some large radius and/or the outflow anticyclone to descend to the surface so that cyclonic relative angular momentum can be diffused into the bulk vortex. As with the foregoing thermodynamic constraints, the net source of cyclonic angular momentum must balance the frictional loss of this quantity exactly. In this context, it is worth pointing out that, in the discussion of their model for a mature hurricane, Carrier *et al.* (1971) suggested that 'a hurricane could last 30 days or more before it used up its angular momentum . . . ', i.e. they presumed that it was not possible to supply enough angular momentum to maintain a steady state. We return to this issue again later.

Together, the above considerations raise questions about a number of previous theoretical and numerical studies of

steady-state hurricanes, including Emanuel's model (Emanuel, 1986, henceforth E86; Emanuel, 1988; Emanuel, 1995; Bister and Emanuel, 1998 and later 'generalizations' by Bryan and Rotunno, 2009a); Wirth and Dunkerton's (2006) comparative study of hurricanes and monsoon circulations and Hakim's 500 day numerical simulations of an axisymmetric hurricane in statistical-equilibrium (Hakim, 2011). They raise also questions regarding a critique by Bryan (2012) of one of our recent articles, who claimed that our solutions after 4 days were not near to a steady state and that a 12 day or more integration was necessary to achieve such a state!

In this article, we examine the constraints imposed by the global angular momentum budget and the vanishing of the spin-up function on the structure of a mature hurricane and discuss the implications for previous studies.

The structure of the article is as follows. To set the scene, we show in section 2 an example of the azimuthally averaged vortex structure of the mature state in an idealized, three-dimensional, numerical simulation of a tropical cyclone. Then, in section 3, we review the equations governing the absolute angular momentum and budgets of this quantity, as well as the constraints on steady balance flow imposed by the spin-up function. Section 4 examines further the simulation discussed in section 2, focusing on the vortex evolution and aspects of the absolute angular momentum field. Section 5 comments briefly on a particular aspect of the simulation requiring further study and section 6 considers the implications of the results for previous studies. Conclusions are presented in section 7.

## 2. An idealized simulation of a mature tropical cyclone

To set the scene for the article, we show kinematic aspects of the mature vortex structure in an idealized numerical model simulation for a tropical cyclone. The simulation relates to the prototype problem for tropical cyclone intensification, which considers the evolution of a prescribed, initially cloud-free axisymmetric vortex in a quiescent environment on an $f$-plane as articulated in Nguyen *et al.* (2008). It is carried out using the numerical model CM1 version 14, a non-hydrostatic and fully compressible cloud model (Bryan and Fritsch, 2002)* in the three-dimensional configuration described by Persing *et al.* (2013), using a stretched horizontal and vertical grid mesh. The inner portion of the mesh (600 × 600 km) has a fixed 3 km horizontal grid spacing. The complete grid mesh of the model domain is 3000 × 3000 km in size and has 260 × 260 grid points.

In brief, the model has prediction equations for the three components of the velocity vector, specific humidity, suspended liquid water, perturbation Exner function and perturbation density potential temperature, where perturbation quantities are defined relative to a prescribed hydrostatic basic state. A simple warm-rain scheme is used in which rain has a fixed fall speed of 7 m s$^{-1}$. For simplicity, ice microphysical processes and dissipative heating are not included. The reference sounding is a nearly moist-neutral sounding generated from the axisymmetric Rotunno and Emanuel (1987) model. The calculations are carried out on an $f$-plane with the Coriolis parameter $f = 5 \times 10^{-5}$ s$^{-1}$, corresponding to 20°N. The surface temperature is 299.6 K (based on the value used in the studies by Rotunno and Emanuel (1987) and Persing and Montgomery (2005)).

Radiative effects are represented by adopting a simple Newtonian cooling scheme capped at 2 K per day, following Rotunno and Emanuel (1987). This scheme serves as a simple expedient for parametrizing the radiative–convective equilibrium process, which operates to maintain the ambient tropical sounding. In choosing this particular set-up, we purposely omit the more complex cloud–radiative feedback processes at infrared wavelengths that have been suggested to accelerate the intensification process (Hakim, 2011; Nicholls and Montgomery, 2013) as well as the negative ocean feedback associated with storm-induced upwelling of colder ocean water below the storm that tends to retard the intensification process (Emanuel *et al.*, 2004).

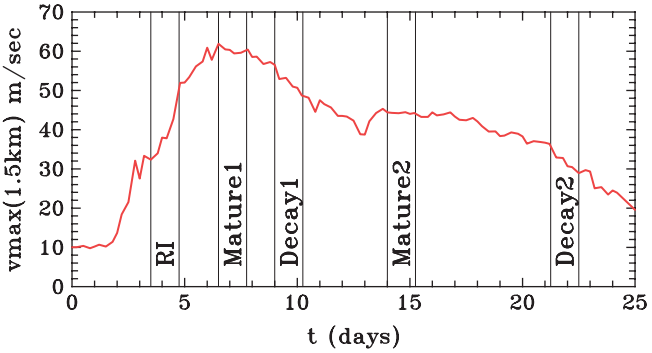


**Figure 1.** Time series of the maximum azimuthally averaged tangential wind component at a height of 1.5 km in the simulation described in section 2.

The outer lateral boundaries are open with a radiative boundary condition (Durran and Klemp, 1983). In order to mitigate the reflection of internal gravity waves from the upper boundary, a Rayleigh damping layer is added at heights above 20 km. In the outflow anticyclone, this damping of horizontal momentum effectively represents an upper-level source of cyclonic relative angular momentum to the vortex, albeit, as we shall see, this source is not sufficient to replenish the cyclonic angular momentum that is lost at the sea surface.

The initial radial and vertical velocity components are set to zero. The initial tangential velocity is taken to be in gradient wind balance with a maximum of 13 m s$^{-1}$ at the surface at a 100 km radius from the centre of circulation. The tangential velocity varies smoothly in space and tends to zero at large radii: it is effectively zero beyond 400 km radius and above $z = 20$ km. The simulation is carried out for a period of 25 days.

Figure 1 shows a time series of the maximum azimuthally averaged tangential wind component at a height of 1.5 km in the foregoing simulation. On the basis of this metric for intensity, the vortex is seen to undergo two periods of rapid intensification, one just after 2 days and the other just after 4 days. It reaches a peak intensity of about 62 m s$^{-1}$ after $6\frac{1}{2}$ days and remains quasi-steady for a little over a day, after which the intensity begins to decline progressively. The decline ceases just before 13 days and after a short period of re-intensification a second quasi-steady period is established, before the final demise. We select five 30 h periods for subsequent analysis, one characterizing the second rapid intensification period (RI in the figure), two characterizing the two quasi-steady periods (mature1 and mature2) and two characterizing the two decay periods (decay1 and decay2). In this section we focus mainly on the mature1 phase, but comment on the other phases later in section 4.

Figure 2 shows radius–height cross-sections of the time-averaged† and azimuthally averaged tangential, radial and vertical‡ velocity components for this simulation during the first mature phase, mature1. Also shown is the corresponding cross-section of the initial tangential velocity component. As is well known (see e.g. Montgomery and Smith, 2014 and references therein), in an azimuthal-mean sense, the radial

*For a complete description of the three-dimensional model and variable definitions, see the technical document 'The governing equations for CM1', available for download at http://www.mmm.ucar.edu/people/bryan/cm1 and also available from G. Bryan at the National Center for Atmospheric Research. For a complete description of the axisymmetric version of CM1, see the article by Bryan and Rotunno (2009b).

†Based on 10 min output data.

‡It is pertinent to point out that both the radial and vertical velocity components exhibit much variability on time-scales of an hour or less and that averaging over 12 h or more is required to obtain a coherent pattern on the vortex scale. This variability is associated predominantly with deep convection and convectively induced (inertia) gravity waves.

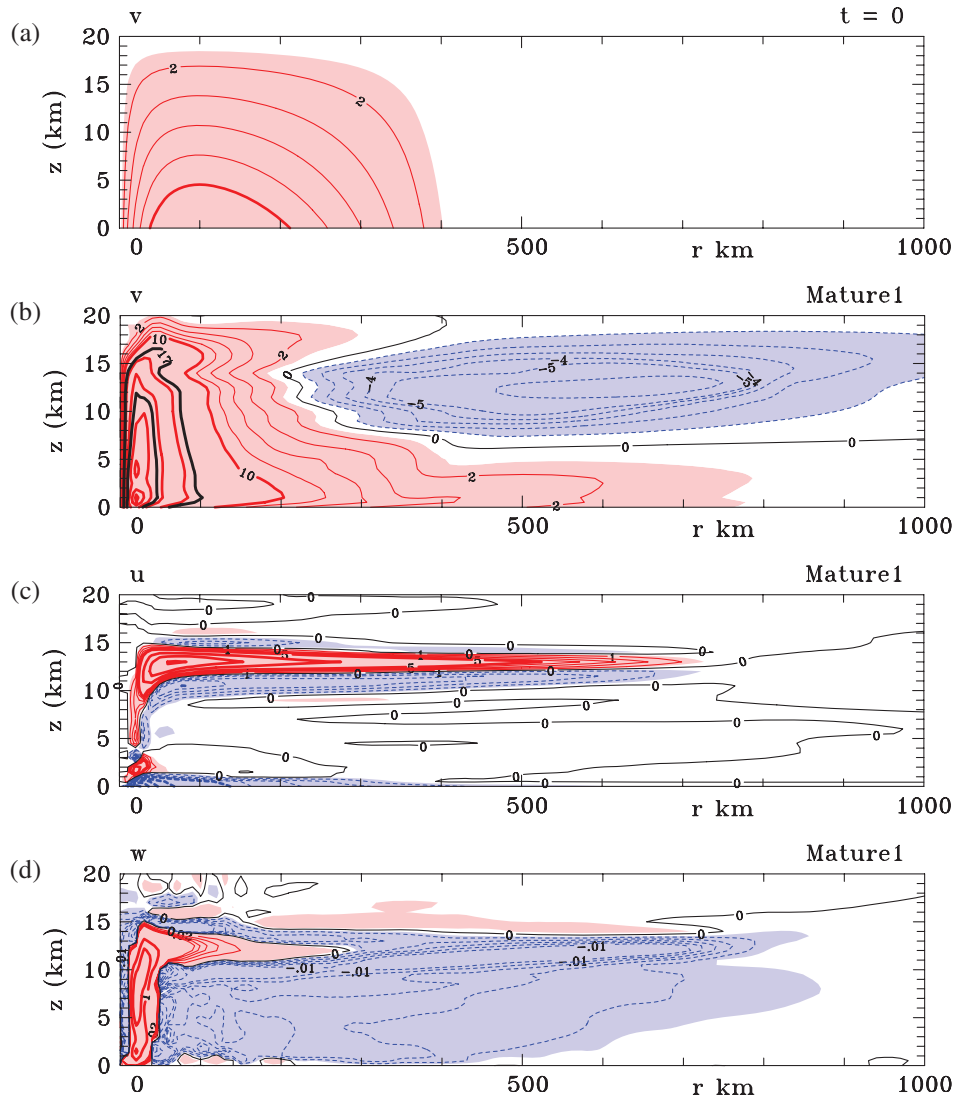


**Figure 2.** Time-averaged radius–height cross-sections showing (a) the initial tangential velocity component, and (b) tangential ($v$), (c) radial ($u$) and (d) vertical ($w$) components of velocity, respectively, in the mature stage of evolution (240–270 h). Contour interval for $v$: thin positive (red in the online article) contours 2–8 m s$^{-1}$; thick positive (red in the online article) contours 10 m s$^{-1}$; thin negative (blue in the online article) contours 1 m s$^{-1}$; the thin (black) line is the zero contour; thick (black) contours have values 17 and 34 m s$^{-1}$, representing approximately gale-force and hurricane force winds, respectively. The online version of the figure shows pink shading for values exceeding 1 m s$^{-1}$ and blue shading for values lower than $-1$ m s$^{-1}$. Contour interval for $u$: thick contours 5 m s$^{-1}$; thin contours 1 m s$^{-1}$; positive contours solid, negative contours dashed. The online version of the figure shows pink shading for values exceeding 0.5 m s$^{-1}$ and blue shading for values less than $-0.5$ m s$^{-1}$. Contours for $w$: thick solid (red in the online article) contours 1 and 2 m s$^{-1}$; thin solid (red in the online article) contours 2–10 cm s$^{-1}$ in steps of 2 cm s$^{-1}$; thin dashed (blue in the online article) contours $-2$ to $-10$ cm s$^{-1}$ in steps of $-2$ cm s$^{-1}$; very thin dashed (blue in the online article) contours $-2$ mm s$^{-1}$ to $-1$ cm s$^{-1}$ in steps of $-2$ mm s$^{-1}$. The online version of the figure shows pink shading for values exceeding 1 mm s$^{-1}$ and blue shading for values less than $-1$ mm s$^{-1}$.

and vertical gradient of latent heating rate associated with the eyewall convection generates an overturning circulation[§] or secondary circulation with, broadly speaking, inflow in the lower troposphere, rising motion in the eyewall cloud, outflow in the upper troposphere and persistent subsidence outside the eyewall region (Figure 2(c) and (d)). In response to this thermal forcing, the tangential wind field amplifies and an anticyclonic circulation develops aloft (compare Figure 2(a) and (b)). The strengthening of the tangential wind at low levels above the frictional boundary layer may be understood in terms of absolute angular momentum conservation in the presence of the overturning circulation (Montgomery and Smith, 2014, section 7.1).

As shown in Figure 1, the quasi-steady state does not persist and the vortex subsequently decays. However, it remains of interest to enquire whether this decay is inevitable, since, as discussed in the Introduction, several purported steady-state solutions have been presented in the literature and the question is as follows: what would be the requirements for the mature state, such as is characterized by the flow fields shown in Figure 2, to be maintained? A further question is this: in what way, if any, do the steady-state solutions referred to in the Introduction differ from the present one?

## 3. Theoretical considerations

To address the questions posed at the end of the preceding section, we examine now certain theoretical concepts that will prove useful for the ensuing discussion.

### 3.1. *Absolute angular momentum*

We consider a vertically aligned, swirling flow on an $f$-plane expressed in cylindrical coordinates $(r, \lambda, z)$ with corresponding azimuthal-mean velocity components $(u, v, w)$ and departures from this mean denoted by primes. The unapproximated continuity equation for the azimuthal-mean flow has the form

$$\frac{\partial \rho}{\partial t} + \frac{1}{r}\frac{\partial \rho r u}{\partial r} + \frac{\partial \rho w}{\partial z} = 0, \qquad (1)$$

where $\rho$ is the density. The azimuthal-mean absolute angular momentum $M$ per unit mass about the vortex axis is defined by

[§]A circulation in the radius-height plane.

the equation

$$M = rv + \frac{1}{2}fr^2, \tag{2}$$

where $f$ is the Coriolis parameter, and $M$ is governed by the equation[¶]

$$\frac{\partial M}{\partial t} + u\frac{\partial M}{\partial r} + w\frac{\partial M}{\partial z} = -\left\langle \frac{1}{\rho}\frac{\partial p'}{\partial \lambda}\right\rangle + E_1 + D, \tag{3}$$

where $p'$ is the pressure perturbation relative to the azimuthal mean and in this equation $\rho$ denotes the total density,

$$E_1 = -\left\langle u'\frac{\partial M'}{\partial r}\right\rangle - \left\langle w'\frac{\partial M'}{\partial z}\right\rangle \tag{4}$$

represents the momentum fluxes associated with eddy processes,

$$D = \frac{1}{r\rho}\frac{\partial}{\partial r}\left[\rho r^3 K_r \frac{\partial}{\partial r}\left(\frac{v}{r}\right)\right] + \frac{1}{\rho}\frac{\partial}{\partial z}\left[\rho K_z \frac{\partial M}{\partial z}\right] \tag{5}$$

represents the unresolved horizontal and vertical diffusive processes and the brackets $\langle \ldots \rangle$ denote an azimuthal average at constant height. Here, $K_r$ and $K_z$ are horizontal and vertical eddy diffusivities, respectively (note that azimuthal variations in eddy diffusivity have been ignored).

From Eq. (3) it follows that, for a steady axisymmetric flow in the absence of eddy fluxes or diffusion,

$$(u, w)\cdot\left(\frac{\partial M}{\partial r}, \frac{\partial M}{\partial z}\right) = 0, \tag{6}$$

i.e. the flow in the meridional plane must be along $M$ surfaces.

With the reasonable anelastic assumption that $\rho = \rho(z)$, the flux form of Eq. (3) is

$$\frac{\partial M}{\partial t} + \frac{1}{r}\frac{\partial ruM}{\partial r} + \frac{1}{\rho}\frac{\partial \rho wM}{\partial z} = E_2 + D, \tag{7}$$

where

$$E_2 = -\frac{1}{r}\left\langle \frac{\partial ru'M'}{\partial r}\right\rangle - \frac{1}{\rho}\left\langle \frac{\partial \rho w'M'}{\partial z}\right\rangle. \tag{8}$$

Integrating the steady-state version of Eq. (7) over a control volume extending from the axis to $r = R$ and from the surface to $z = H$ and using the boundary conditions that $u = 0$ at $r = 0$, $w = 0$ at $z = 0$ and $z = H$, and assuming that $\partial M/\partial z = 0$ at $z = H$, gives

$$\int_0^H \left[\rho ruM + \langle \rho ru'M'\rangle\right]_{r=R} \mathrm{d}z = -\int_0^R \left[\rho K_z \frac{\partial M}{\partial z}\right]_{z=0} r\,\mathrm{d}r + \int_0^H \left[\rho K_r r^3 \frac{\partial}{\partial r}\left(\frac{v}{r}\right)\right]_{r=R} \mathrm{d}z. \tag{9}$$

It follows that, when $R$ is sufficiently large, $u$ is essentially zero,[‖] so that $[\rho uM]_{r=R}$ is relatively small compared with the other terms in Eq. (9). Thus, the only possible sources of $M$ to maintain the system in a steady state could be the radial diffusion of cyclonic angular *velocity*[**] at $r = R$ at heights where the flow is anticyclonic (the second term on the right of Eq. (9)), the vertical diffusion at the ocean surface at radii where the flow is anticyclonic (contained in the first term on the right of Eq. (9)) or a positive eddy flux of tangential momentum at $r = R$ (through the term $\left[\langle \rho ru'M'\rangle\right]_{r=R}$). Given the vanishing of the radial mean influx of $M$ at $r = R$, it is important to note that *nowhere does the planetary angular momentum enter the angular momentum balance for the vortex system*. In other words, Eq. (9) implies that the global amount of planetary angular momentum within the control volume does not change with time, so that *it would be misleading to think of the Earth's background rotation as representing an unlimited supply of angular momentum to the storm*.

The structure and evolution of the $M$ surfaces in the simulation described in section 2 are discussed in section 4.

### 3.2. *Balanced flow evolution and the spin-up function*

For a vortex evolving slowly according to axisymmetric balance dynamics, one can derive a diagnostic equation for the stream function of the axisymmetric overturning circulation, or alternatively for the geopotential tendency, $\partial\Phi/\partial t$, in terms of the processes that are tending to drive the vortex away from balance, such as the diabatic heating rate and frictional and eddy processes (Shapiro and Willoughby, 1982; Shapiro and Montgomery, 1993; Vigh and Schubert, 2009). The equation for the stream function of the overturning circulation is often referred to as the Sawyer–Eliassen equation and a derivation of it for an axisymmetric flow is given, for example, by Montgomery and Smith (2014: see section 2.3). However, in a strict steady state, the steps taken to derive the Sawyer–Eliassen equation become degenerate because the time tendencies of $v$ (or $M$) and the potential temperature, $\theta$, that are eliminated in the derivation are identically zero.

The use of the geopotential tendency equation for describing the balanced evolution of a vortex has a number of advantages over the use of the Sawyer–Eliassen equation. To begin with, unlike the Sawyer–Eliassen equation, the derivation is not degenerate for the steady state. A mathematical advantage of using the geopotential tendency equation is that it avoids the need first to invert for the overturning circulation, then to advect $M$ by the radial and vertical flow and finally to link the changes in $M$ to changes in the mass field of the vortex by solving the thermal wind equation. In fact, the geopotential tendency equation gives a direct link between the heat and momentum forcing to the changes in the mass field. Persing *et al.* (2013) have shown that this equation provides a useful framework for comparing balanced aspects of the spin-up of three-dimensional and axisymmetric model hurricanes. As shown by Shapiro and Montgomery (1993; their Eq. (4.10)), the geopotential tendency equation is a compact form of the balanced perturbation potential vorticity equation in which the radial and vertical advection of the basic state potential vorticity are implicit.

[¶]On a $\beta$-plane, there would be an additional term $-\frac{3}{2}\beta r^2\langle u' \sin\lambda\rangle$ on the right-hand side of this equation.

[‖]According to axisymmetric balance dynamics (Ooyama, 1969; Shapiro and Willoughby, 1982), the amplitude of the overturning circulation outside the imposed heat source region (the eyewall) will decay exponentially with distance on a scale given by the local Rossby radius of deformation for the axisymmetric vortex, $L_R = (NH)/I$, where $N$ is the Brunt–Väisälä frequency, $H$ is the effective vertical scale of the heating-rate forcing, $I^2 = (f + \zeta)(f + 2v/r)$ is the inertial (centrifugal) stability of the axisymmetric vortex and $\zeta = \partial v/\partial r + v/r$ the relative vertical vorticity at radius $r$. If we make the reasonable assumption that the heating is dominated by the convective mode, then, $H \equiv H_{\mathrm{trop}}/\pi$, where $H_{\mathrm{trop}}$ is the height of the convective cloud tops (the tropopause height: Gill, 1980). This property of the balanced overturning circulation implies that the azimuthally averaged radial velocity decays exponentially at several Rossby radii. Near the eyewall region, $L_R \sim 60$ km (Shapiro and Montgomery, 1993); it increases rapidly to several hundred km outside the eyewall. *The net result is that the mean radial inflow in the lower and middle troposphere becomes practically zero at radii as small as 500 km and cannot supply planetary angular momentum to the system.*

[**]Note that angular momentum is not diffused radially in the tangential momentum equation, but rather angular velocity, $v/r$.

Following Vigh and Schubert (2009), the geopotential tendency equation may be written as

$$L\frac{\partial \Phi}{\partial t} = S, \tag{10}$$

where $L$ is a linear, second-order, partial differential operator in the radius-height plane and

$$S = \eta \cdot \nabla \left(\frac{\dot{\theta}}{P}\right)_{M=\text{constant}}, \tag{11}$$

where the azimuthal mean quantities $\eta$, $\theta$, $\dot{\theta}$, $P$ and $S$ are the absolute vorticity vector, potential temperature, material derivative of $\theta$ i.e. the net diabatic heating rate, Rossby–Ertel potential vorticity and spin-up function, respectively.

If the flow is symmetrically stable, the partial differential equation (10) is elliptic with a forcing term that is equal to the scalar product of $\eta$ and the vector gradient of $\dot{\theta}/P$ along an $M$ surface. Vigh and Schubert refer to $S$ as the *cyclogenesis function*, but we prefer the term 'spin-up function', as cyclogenesis is observed to be distinctly non-axisymmetric (see e.g. Montgomery *et al.*, 2012 and references therein).

In axisymmetric balance dynamics, for a globally steady flow, the spin-up function must be identically zero, at least in regions where diffusive effects (subgrid-scale processes modelled via downgradient diffusion parametrization, etc.) are sufficiently small. This condition provides a constraint on the secondary circulation in terms of the primary circulation and the diabatic heating (and, in general, other forcing terms). Although the requirement of continuity (Eq. (1)) imposes a further constraint, this, together with the vanishing of the spin-up function, does not provide a means to determine the steady-state primary circulation and mass field. The constraint that $S = 0$ neglects the typically small effects of eddy angular momentum fluxes and does not apply in the boundary layer, where the flow is not governed consistently by balance dynamics.

### 3.3. *Another issue concerning a hypothetical, analytical steady-state solution*

Although the prior two subsections have identified two important constraints that need to be satisfied for a steady-state hurricane to exist, the second one is only formally applicable above the frictional boundary layer, where the flow evolves approximately via balance dynamics. The linking of this constraint with the boundary-layer flow presents a challenge in the construction of a hypothetical steady-state theory for a tropical cyclone. The problem is that the top of the boundary layer is open. At radii where there is ascent out of the boundary layer, an open boundary condition is required to allow, *inter alia*, the high tangential wind speeds that are spun up in the boundary layer to be lofted into the interior flow. The formulation of such a condition is problematic, as discussed by Smith and Montgomery (2010), and it seems wrong to us to constrain the flow to return to a *prescribed* gradient wind, as is typically assumed in steady boundary-layer theory. Such a prescription at an outflow boundary makes the physical problem ill-posed, as the boundary layer itself should be allowed to determine the tangential momentum that it expels into the bulk vortex aloft (see also Rotunno and Bryan, 2012, p. 17).

## 4. Vortex evolution in the prototype problem for intensification

### 4.1. *Overview*

We consider now dynamical aspects of the vortex evolution in the simulation described in section 2. Figure 3 shows Hovmöller diagrams of the tangential wind speed and $M$ surfaces as functions of radius at heights of 1.5 and 12 km in the simulation, while Figure 4 shows time series of the maximum and minimum values of tangential wind speed at a height of 12 km. Contours representing gale-force winds ($17\,\mathrm{m\,s^{-1}}$) and hurricane-force winds (about $34\,\mathrm{m\,s^{-1}}$) are highlighted in Figure 3 by thick black lines. Each panel of Figure 3 shows also the five time periods defined in Figure 1. For these calculations, the origin of the cylindrical coordinate system is defined as the minimum of the time-averaged surface pressure. The averaging interval for the surface pressure field on the high-resolution subdomain is the nominal time $\pm 3$ h. During the first rapid intensification period to about 4 days, the vortex expands in size, as measured by the increase in the radius of gale-force winds (Figure 3(a)). Thereafter, while the radius of hurricane-force winds continues to expand until about 6 days, the radius of gales begins to decline steadily. This behaviour is not typical of all calculations that we have examined and in some cases the radius of gale force winds continues to increase after the vortex has reached its peak intensity. The expansion of the wind field during the first few days of the foregoing calculation is accompanied, of course, by an inward movement of the $M$ surfaces and as the winds decline these surfaces move outwards again (Figure 3(b)).

The evolution of the $M$ surfaces is determined not only by the radial advection of $M$, but also by its vertical advection, eddy angular momentum fluxes and, to a lesser extent above the boundary layer, the turbulent diffusion of tangential momentum. The effects of the vertical advection of $M$ are seen clearly in the corresponding Hovmöller diagrams at a height of 12 km. The tangential wind speed is initially cyclonic at this altitude (Figure 3(c)) but, as outflow begins, there is a brief period after about 2 days when the flow is anticyclonic at all radii. This period corresponds to a rapid outward movement of the $M$ surfaces shown in Figure 3(d). Thereafter, as cyclonic angular momentum is advected upwards in the inner-core convective plume, the flow becomes cyclonic once again at inner radii, but the anticyclone progressively strengthens and spreads radially outwards until about 9 days. After this time, the strength and radial extent of both the upper-level cyclone and anticyclone steadily decrease. Of course, the decrease in the strength of the anticyclone corresponds to an inward movement of the $M$ surfaces seen in Figure 3(d).

It is pertinent to remark that the ability to draw $M$ surfaces inwards depends, *inter alia*, on the strength of the convective forcing, as demonstrated in Persing *et al.* (2013).

We show now the distribution of $M$ in the $r$–$z$ plane (Figure 5). Figure 5(a) shows the initial distribution of $M$ in this plane. Since the initial tangential wind is confined largely to radii less than 400 km (Figure 2(a)), the $M$ surfaces beyond this radius are dominated by the planetary contribution, $\frac{1}{2}fr^2$, and are therefore essentially vertical. Inside 400 km, the initial $M$ surfaces are distorted by the relative angular momentum contribution $RAM = rv$, which has, of course, vertical structure. The outermost $M$ surfaces are coloured red in the online version of the figure to highlight their radial displacement as the vortex matures.

Figure 5(b) shows the $r$–$z$ distribution of the $M$ surfaces averaged over the first mature period in Figures 1 and 3. As the overturning circulation develops, the $M$ surfaces move radially inwards in the lower troposphere and radially outwards in the upper troposphere. As discussed in section 3, where the surfaces move inwards above the boundary layer, the local tangential circulation increases and where they move outwards the tangential circulation decreases. Indeed, where the surfaces move outwards beyond their potential radius,[††] the tangential wind component becomes anticyclonic.

Figure 6 shows the distribution of relative angular momentum $RAM$ for the two mature and two decay phases. Significantly,

[††] The *potential radius* is the radius at which an air parcel, if displaced radially while conserving its absolute angular momentum, would have zero tangential wind speed.

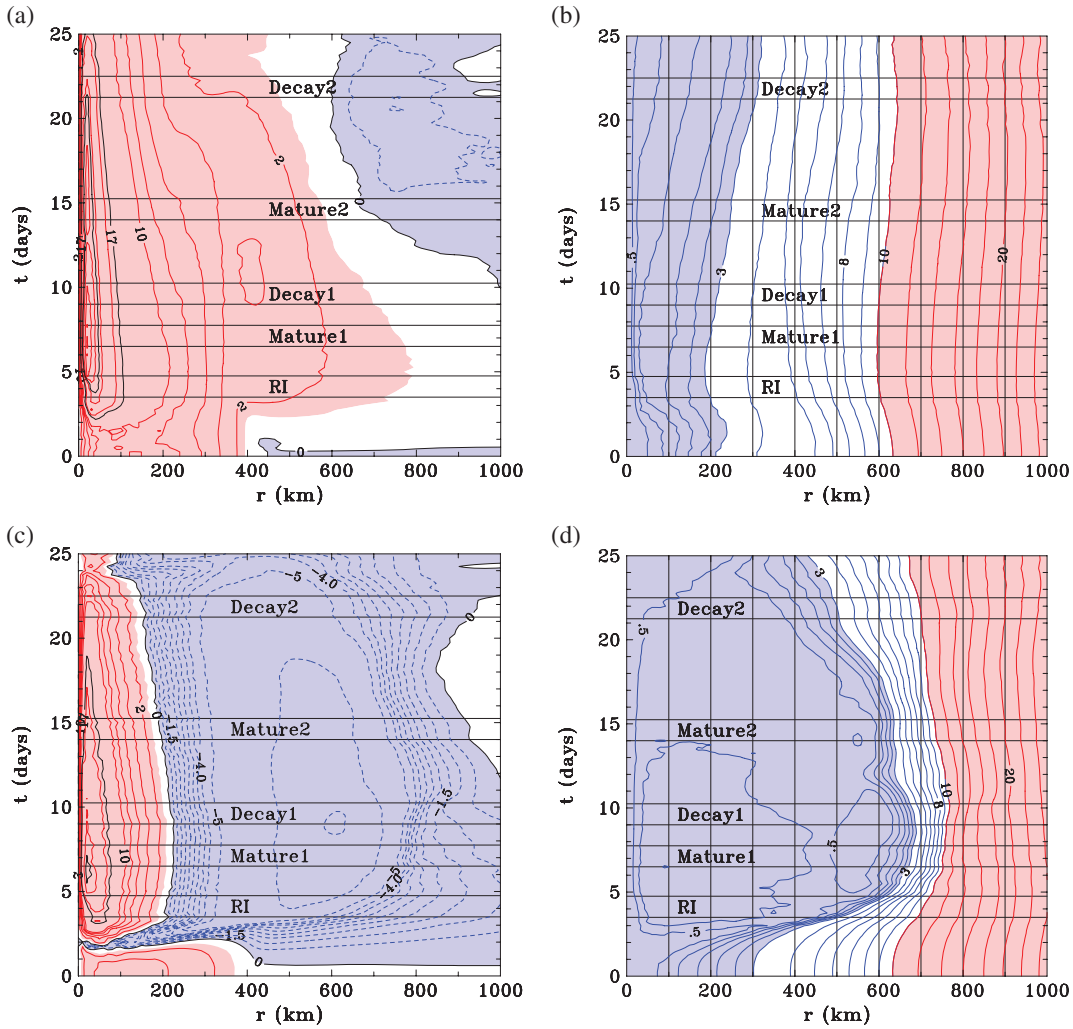


**Figure 3.** Hovmöller time–radius plots of (a) $v$ at a height of 1.5 km and (b) the corresponding $M$ surfaces at this level. Panels (c) and (d) show the corresponding fields at a height of 12 km. Contour interval for $v$: thin positive (red in the online article) contours 2–8 m s$^{-1}$; thick positive (red in the online article) contours 10 m s$^{-1}$; thin negative (blue in the online article) contours 1 m s$^{-1}$; the thin (black) line is the zero contour; thick (black) contours have values 17 and 34 m s$^{-1}$, representing approximately gale-force and hurricane force winds, respectively. In the online version of the figure, pink shading indicates values exceeding 1 m s$^{-1}$, blue shading values less than $-1$ m s$^{-1}$. Contour interval for $M$: $0.5 \times 10^6$ m$^2$ s$^{-1}$ to $3 \times 10^6$ m$^2$ s$^{-1}$, then $1 \times 10^6$ m$^2$ s$^{-1}$ to $1 \times 10^7$ m$^2$ s$^{-1}$, then $2 \times 10^6$ m$^2$ s$^{-1}$. The region with $M \leq 3 \times 10^6$ m$^2$ s$^{-1}$ is shaded blue in the online article; that with $M > 1 \times 10^7$ m$^2$ s$^{-1}$ is shaded pink.

although the upper anticyclone descends progressively as the vortex evolves, at no stage does it extend down to the surface: in fact, in the second decay phase its minimum altitude still lies above 3 km. The reason seems to be that, on grounds of mass continuity, the amount of mass exiting a cylindrical control volume of radius $R_c$ must be approximately balanced by a comparable amount of mass entering it.[‡‡] Thus, the outflow that leads to the outward radial advection of $M$ surfaces in the upper troposphere and to the formation of the upper anticyclone must be approximately compensated for at other altitudes by radial inflow, which tends to promote spin-up. This feature can be seen in Figure 5(b), wherein, at a given radius, the $M$ surfaces bow outwards at some altitudes and inwards at others. Of course, the local rate of change of $M$, $\partial M/\partial t$, is influenced, *inter alia*, by both radial and vertical advection of $M$ and since $\partial M/\partial r$ is typically positive and $\partial M/\partial z$ is typically negative throughout the free troposphere, inflow will tend to increase $M$ locally, while subsidence will tend to decrease it.

It is interesting to note that by the second mature phase, a surface-based anticyclonic flow has formed at large radii ($> 500$ km) and has strengthened by the decay phase. This formation is associated with the development of a weak radial outflow at these levels, below the low- to mid-tropospheric inflow under the outflow layer (not shown). Significantly, the shallow anticyclone forms separately from the upper anticyclone and underlies a region of cyclonic circulation that arises from middle-tropospheric inflow associated with the return branch of the outflow. Although this anticyclone represents a means for diffusing cyclonic angular momentum into the system as a whole, the fact that the vortex decays is evidence that any addition of cyclonic angular momentum at these radii is not sufficient to maintain the vortex.

As a point of clarification, we are not arguing that the decline in the maximum tangential wind in the vortex core is *immediately attributable* to the lack of an adequate source of

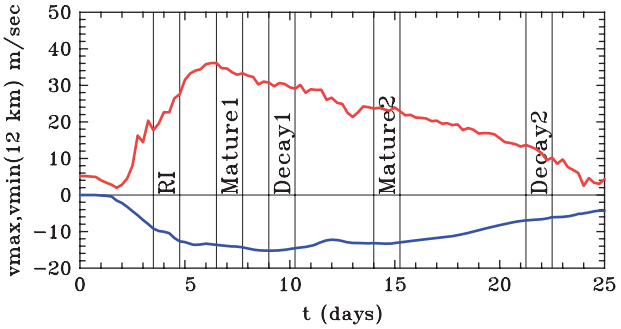


**Figure 4.** Time series of the maximum and minimum azimuthally averaged wind component at a height of 12 km in the simulation described in section 2.

[‡‡]There may be a small difference between the mass entering the control volume and that leaving, consistent with the change in mean surface pressure within the control volume.

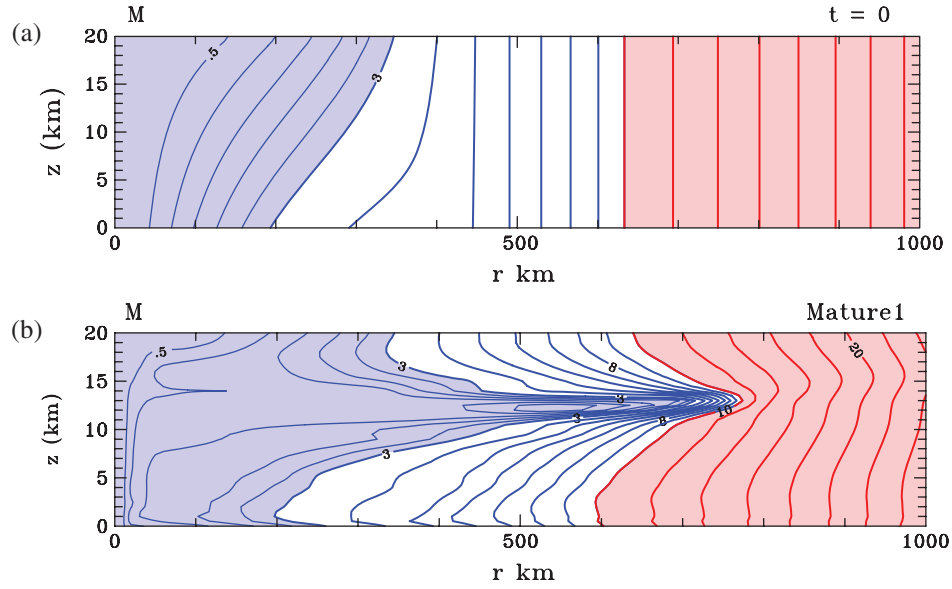


**Figure 5.** Radius–height cross-sections of the $M$ surfaces in (a) the initial state and (b) the first mature state (cf. Fig. 1). Contour interval: inner region (blue shaded in the online article) $0.5 \times 10^6$ m$^2$ s$^{-1}$ to $3 \times 10^7$ m$^2$ s$^{-1}$; middle unshaded region, interval $1 \times 10^6$ m$^2$ s$^{-1}$ to $1.0 \times 10^7$ m$^2$ s$^{-1}$; outer (pink shaded in the online article) region, interval $5 \times 10^6$ m$^2$ s$^{-1}$).

cyclonic angular momentum to the system. However, the lack of such a source would have to be the ultimate cause of decay. A preliminary analysis suggests that the initial decline in intensity is a consequence of the progressive stabilization of the inner core to deep convection so that the convective mass flux is no longer sufficient to ventilate all the air that is converging in the boundary layer. Animations of the model output data show that this inability of deep convection to ventilate the boundary-layer inflow leads to outflow immediately above the inflow layer, with a consequent spin-down of the tangential winds in a layer immediately above the inflow layer. This aspect of the spin-down process is currently under investigation as part of a separate study and the results will be submitted for publication in due course.

### 4.2. *Angular momentum tendency in the mature stage*

As the theme of the article concerns the possible existence of a global steady state, it is enlightening to digress and examine the terms in the time-mean, azimuthally averaged, angular momentum tendency equation, i.e. the equation for $\partial M/\partial t$, during the mature states. On the reasonable assumption that the radial and vertical diffusive contributions to $\partial M/\partial t$ are small in the free troposphere, we show in Figure 7 the contributions of radial, vertical and total advection to $(\partial M/\partial t)_{\rm adv}$ during the first mature stage of development, as well as the diagnosed distribution of total tendency, $(\partial M/\partial t)_{\rm tot}$.

The radial advective tendency of $M$ is large and positive in a shallow layer adjacent to the surface and strongly negative in most of the eyewall updraught, except in the inertial recoil region,[§§] which is most prominent in the altitude range between 3 and 5 km (Figure 7(a)). Elsewhere, this tendency is very weakly positive through an appreciable portion of the lower half of the troposphere, but has a layered structure in the upper troposphere, with alternating regions of positive and negative tendency. The major signal in the upper troposphere is a dipole pattern of elevated positive and negative values where the upper anticyclone continues to evolve.

The vertical advective tendency of $M$ is similar in structure to the radial tendency, but largely opposite in sign (Figure 7(b)) so that the total advective tendency indicates considerable cancellation (Figure 7(c)). This near-cancellation is to be expected because, to a first approximation, $M$ is materially conserved following the azimuthal mean overturning circulation. However, there is further cancellation when the eddies and subgrid-scale tendencies are taken into account (Figure 7(d)). As shown in Persing *et al.* (2013), the subgrid-scale tendencies are largest in the boundary layer and largely oppose the advective tendency there in the mature phase, while above the boundary layer the tendencies result largely from the eddies.[¶¶]

The total tendency of $M$ during the mature stage is close to zero in the inner-core region (Figure 7(d)), which is consistent with our definition of a quasi-steady state. However, the total tendency outside the core region shows vertical structure, with regions of weak positive and negative values. The negative regions are more extensive, suggesting a general tendency for angular momentum to be lost in the outer circulation. This feature is consistent, of course, with the decline in vortex intensity and size indicated in Figure 3. It is also consistent with the behaviour of integrated *RAM* discussed below.

### 4.3. *Integrated RAM and KE*

Questions that arise naturally from the foregoing analyses are as follows: how are the domain-integrated, mass-weighted *RAM* and domain-integrated kinetic energy (*KE*) partitioned between cyclonic *KE* (*cKE*) and anticyclonic *KE* (*aKE*) and how does the partitioning vary with time? To answer these questions, we show in Figure 8 time series of these integrals,[‖‖] normalized by their respective initial values, noting that the initial vortex is entirely cyclonic. There is a progressive loss of integrated cyclonic *RAM* as the system spins up and matures (Figure 8(a)). Moreover,

[§§] In essence, this 'inertial recoil' effect is a standing centrifugal wave, which is damped as the air ascends into the eyewall and the tangential wind and radial pressure gradient come into gradient balance above the boundary layer (Smith *et al.*, 2009, section 4.2; Persing *et al.*, 2013).

[¶¶] Persing *et al.* (2013) also showed that the eddy momentum fluxes are generally not downgradient.

[‖‖] The quantities *RAM* and *KE* are defined by the formulae

$$RAM = 2\pi \int_{r=0}^{1000\ \rm km} r\,{\rm d}r \int_{z=0}^{25\ \rm km} \rho r v\,{\rm d}z$$

and

$$(cKE,\, aCE) = 2\pi \int_{r=0}^{1000\ \rm km} r\,{\rm d}r \int_{z=0}^{25\ \rm km} (A,B)\rho(u^2+v^2+w^2)\,{\rm d}z,$$

where $(A, B) = 1$, except $A \equiv 0$ if $v < 0$ and $B \equiv 0$ if $v > 0$.

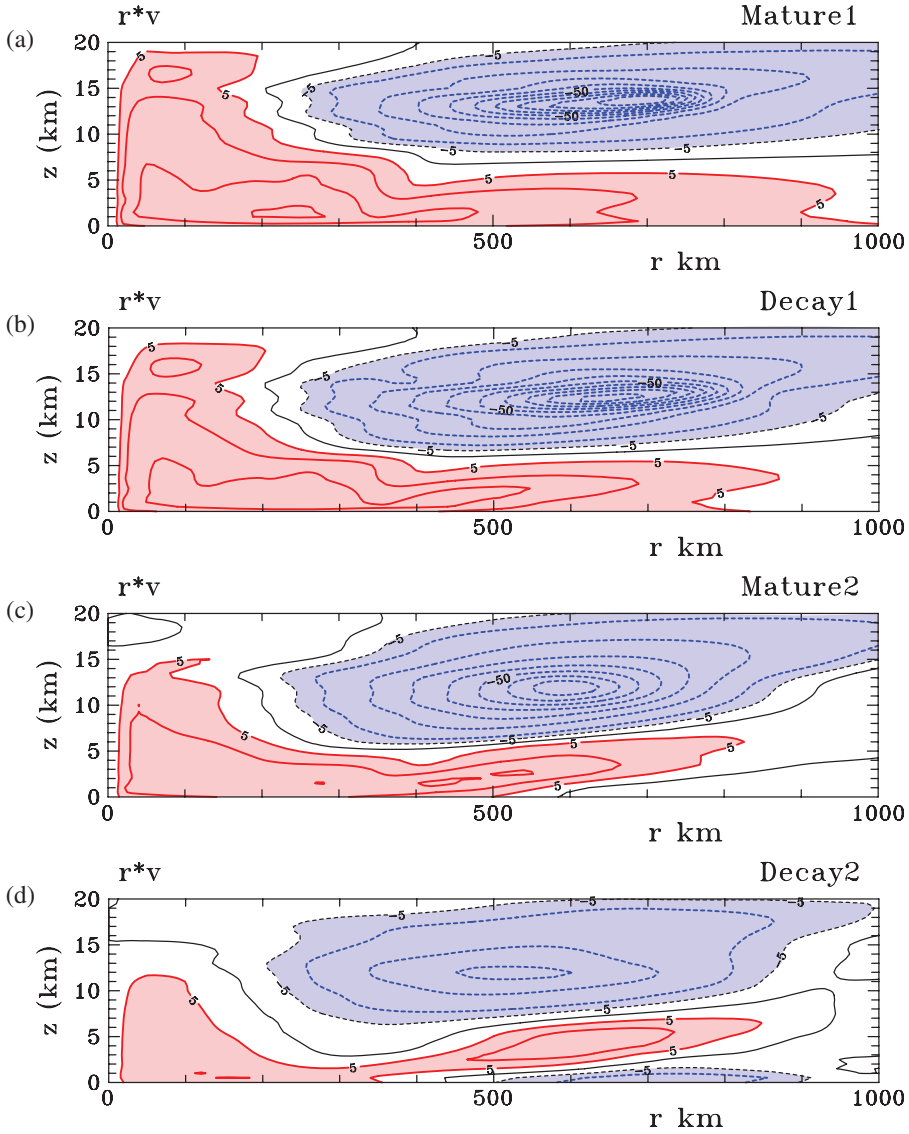


**Figure 6.** Radius-height cross-sections of the relative angular momentum $r \times v$ surfaces in (a) the first mature state, (b) the first decay phase, (c) the second mature phase and (d) the second decay phase. Contour interval: $5.0 \times 10^5$ m$^2$ s$^{-1}$. Solid contours are cyclonic, dashed contours anticyclonic. The thin solid contour is the zero contour. Regions with contour values in excess of the contour interval in magnitude are shaded pink (positive values) and blue (negative values) in the online article.

the integrated *RAM* becomes negative at close to 5 days, more than a day before the vortex reaches its maximum intensity (see Figure 1). Subsequently, the integrated *RAM* becomes strongly negative, more so in magnitude than its initial value, with only a small trend back to zero at long times. The weak trend to reduce the negative *RAM* is due presumably to both the diffusion of cyclonic *RAM* in the weak anticyclonic surface flow at large radii and the artificial relaxation of the flow to a state of zero horizontal flow near the upper boundary.

Figure 8(b) shows the time evolution of *cKE* and *aKE*, normalized by the initial value of *cKE*. For the first day and a half, *cKE* declines before increasing as the vortex intensifies. It reaches a peak of nearly 2.5 times its initial value after 6 days, when the vortex intensity is at its peak. Thereafter it declines progressively to somewhat less than half its initial value after 25 days. In contrast, *aKE* remains close to zero until the vortex starts to intensify and then it increases, reaching a peak after about $9\frac{1}{2}$ days when the upper anticyclone reaches its peak intensity (see Figure 4). After a brief period of decline, *aKE* increases again, reaching a peak marginally less than the first at about $15\frac{1}{2}$ days, before finally declining. Although the peak value of *cKE* is about 50% larger than that of *aKE*, the magnitude of *aKE* exceeds that of *cKE* between 14 and 21 days as the vortex decays. As far as we are aware, the foregoing analysis is the first to quantify the relative amount of kinetic energy in the outflow anticyclone.

## 5. Upper-level inflow jets

A prominent feature of the radial velocity component shown in Figure 2(c) is the layered structure of inflow and outflow in the upper troposphere, where the symmetric stability is weak or the flow is symmetrically unstable (Bui *et al.*, 2009). The regions of upper-tropospheric inflow tend to be co-located with ones of subsiding motion (Figure 2(c)) and may be a manifestation of inertial instability in the outflow layer. This layered structure is a feature of both the mature and decaying phases. We have found a similar feature in other calculations using a different model and are investigating the role of the inflow jets above and below the main outflow. We will report on this investigation separately in due course.

## 6. Implications for previous studies

We have shown just one three-dimensional, convection-permitting simulation together with supporting diagnostic analyses and interpretations for the prototype problem for tropical cyclone intensification. However, it is our experience that the behaviour described in sections 2, 4 and 5 is typical of other extended-period integrations in the sense that, after a period of maturity, the vortices decay. While the inability of the absolute angular momentum loss at the surface to be replenished may be only one factor in the subsequent decay of the vortex, the

 

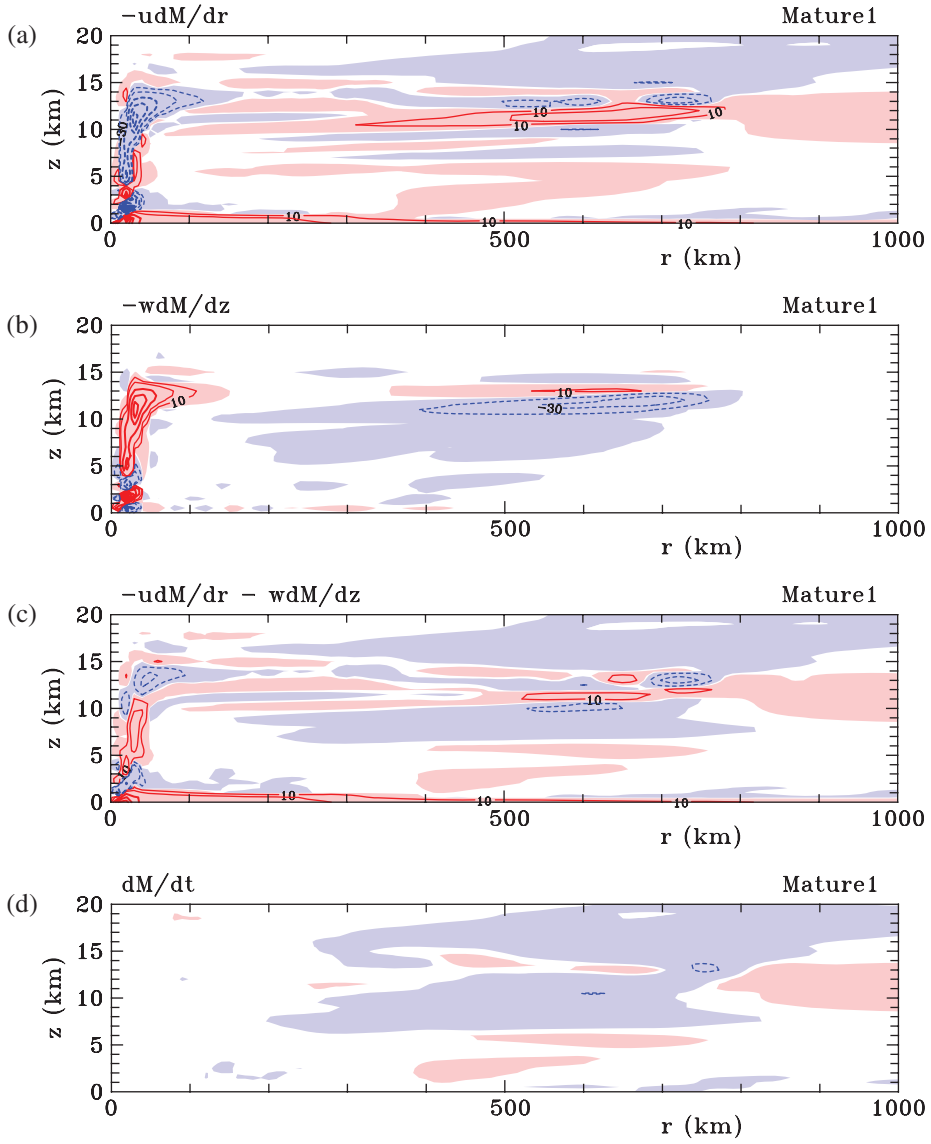


**Figure 7.** Radius–height cross-sections of selected terms in the azimuthally averaged tendency equation for $M$ during the first mature stage: (a) mean radial advection ($-u\partial M/\partial r$), (b) mean vertical advection ($-w\partial M/\partial z$), (c) mean total advection ($-u\partial M/\partial r - w\partial M/\partial z$) and (d) the diagnosed time tendency $\partial M/\partial t$. Contour levels: thick contours 100 $m^2\ s^{-2}$; thin contours have values $\pm 10$ and $\pm 30$ $m^2\ s^{-2}$. Solid contours have positive values, dashed contours negative values. Regions with tendency $\leq 1$ $m^2\ s^{-2}$ are shaded blue in the online article; those with tendency $\geq 1$ $m^2\ s^{-2}$ are shaded pink.

collapse of convective forcing in the primary eyewall region being another, we believe it to be an important one. In this section, we examine four previously published studies of purportedly steady-state tropical cyclone models (or simulations), focusing on the structure of the $M$ surfaces and the source of absolute angular momentum required to maintain the steady state. These studies include the steady-state models of E86 and Wirth and Dunkerton (2006), the statistical equilibrium model of Hakim (2011) and the advocated need for 12 day numerical integrations to achieve a quasi-steady state (Bryan, 2012).

### 6.1. *Emanuel's model*

In what became a highly influential article, E86 developed a steady-state model for a mature hurricane that subsequently led to a major paradigm shift in the theory for the intensification of these storms (see Montgomery and Smith, 2014 for a contemporary review and the role of this model in related intensification theory). A sketch of the model is shown in Figure 9. Briefly, the hurricane vortex is assumed to be steady and circularly symmetric about its axis of rotation and in gradient and hydrostatic balance. The boundary layer is taken to have uniform depth, $h$, and is divided into three regions. Regions I and II encompass the eye and eyewall, respectively, while Region III refers to that beyond the radius, $r_m$, of maximum tangential wind speed, $v_m$, at the top of the boundary layer. E86 takes the outer radius of Region II to be $r_m$ on the basis that precipitation-driven downdraughts may be important outside this radius, but recent observations show it is closer to the inner edge (Marks *et al.*, 2008, their figure 3). When they exit the boundary layer, air parcels are assumed to rise to the upper troposphere, conserving their $M$ and saturation pseudo-equivalent potential temperature, $\theta_e^*$.

Above the boundary layer, the $M$ and $\theta_e$ surfaces, which are congruent, are assumed to flare outwards with height and become almost horizontal in the upper troposphere. Emanuel (2003, p. 83) notes that 'Air descends in the distant environment ... where the entropy acquired in the inflow leg is lost by electromagnetic radiation to space, and angular momentum is gained by mixing with the environment. This leg is nearly isothermal. ... The cycle is closed by an angular-momentum-conserving leg between points o′ and a .... ', where $v$ is assumed to be zero at the top of the boundary layer and at the surface. Here, the points o′ and a are shown in Figure 9, for the particular $M$ surface descending to the point at the lower surface at which $v = 0$ (the curve running from o′ to a). Outside this sloping surface, the tangential winds are assumed to be identically zero and thus $M$ increases with radius according to $fr^2/2$. At all radii outside the $M$ surface (o′–a), the $M$ surfaces are vertical until they intersect with the sloping $M$ surface (o′–a), whereupon there is a discontinuity of $M$ between the value on the sloping surface and values just below it. The

 

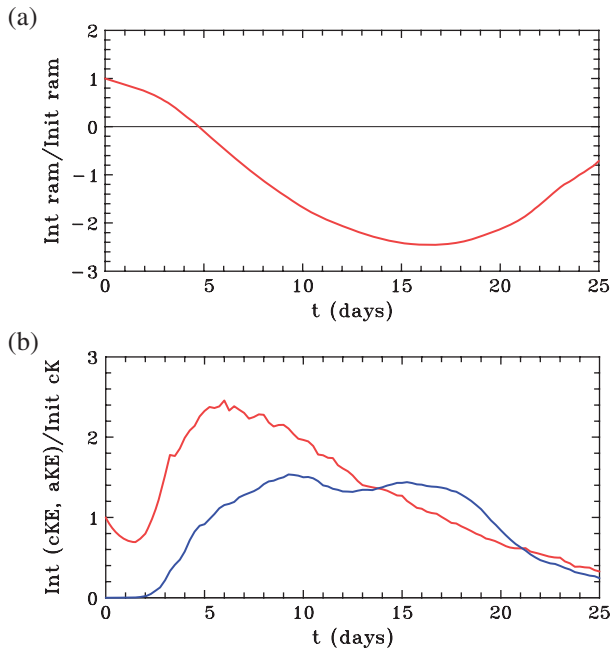


**Figure 8.** Time series of (a) the mass-weighted integral of azimuthally averaged *RAM* normalized by the initial value and (b) the mass-weighted kinetic energy of cyclonic flow (*cKE*, where $v > 0$) and anticyclonic flow (*aKE*, where $v < 0$) normalized by the initial value, respectively. In both (a) and (b), the integration domain is over the entire vortex system defined by the region (0, 1000 km) × (0, 25 km).

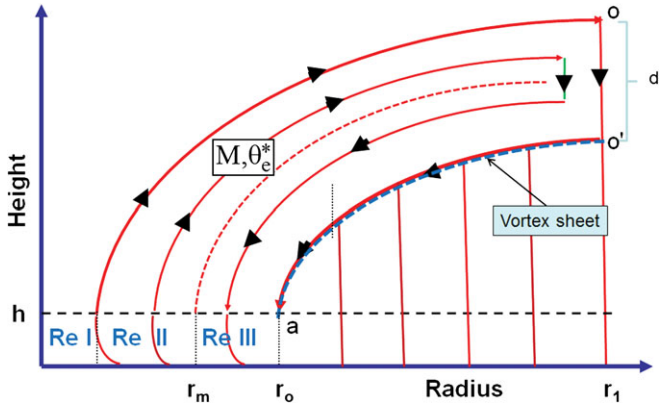


**Figure 9.** Schematic diagram of the Emanuel (1986) model for a steady-state mature hurricane. The boundary layer is assumed to have constant depth $h$ and is divided into three regions as shown: the eye (region Re I), the eyewall (region Re II) and outside the eyewall (region Re III), where spiral rainbands and shallow convection emanate into the vortex above. The model assumes that the radius of maximum tangential wind speed, $r_m$, is located at the outer edge of the eyewall cloud, whereas recent observations (e.g. figure 3 of Marks *et al.*, 2008) indicate that it is closer to the inner edge. The arrows indicate the direction of the overturning circulation. The absolute angular momentum per unit mass, $M$, and pseudo-equivalent potential temperature, $\theta_e$, of an air parcel are conserved after the parcel leaves the boundary layer and ascends in the eyewall cloud. The precise values of these quantities depend on the radius at which the parcel exits the boundary layer. The middle dashed curve emanating from $r_m$ is the $M$ surface along which the vertical velocity is zero and demarcates the region of ascent in the eyewall from that of descent outside the eyewall. The outer dashed curve indicates the location of the vortex sheet described in the main text. The flow segment between **o** and **o′** represents the location at which air parcels are assumed to descend while cooling by infrared radiation to space and gaining relative angular momentum from the environment.

discontinuity in $M$ along this surface implies a singular sheet of absolute vorticity pointing downwards, but generally not parallel with the surface. The eye is assumed to be in solid body rotation and borders an outward-sloping $M$ surface. Since the distribution of $M$ varies continuously between the outer eye and the eyewall region, there does not appear to be a singular sheet of absolute vorticity along the bordering $M$ surface.

We know that the E86 model and its later embellishments have fundamental limitations in the formulation of the boundary layer, as discussed by Smith *et al.* (2008). However, there remain unanswered questions about the far-field flow characteristics of this steady-state solution. For example, what determines $r_1$ and the amount of subsidence that occurs? By our understanding, $r_1$ and the amount of subsidence seem to have been chosen so that the only supply of angular momentum is from the upper troposphere, presumably in the form of cyclonic eddy angular momentum fluxes and their divergence (see Eq. (9)). However, had the $M$ surface (o′–a) been chosen to have a negative $v$ at the surface, there would have been a supply of cyclonic angular momentum at the surface for $r > r_o$. This scenario would correspond to the descent of the upper anticyclone to the surface, as discussed in section 3.1.

Another question is this: what are the implications of the outer vortex sheet in terms of the force fields that must maintain it? Finally, it has yet to be demonstrated that this hypothetical configuration is consistent with the vanishing of the spin-up function as discussed in section 2.

The foregoing questions apply to all versions of Emanuel's steady-state theory and generalizations thereof referenced in the Introduction, including those providing an estimate for the maximum potential intensity of tropical cyclones (Emanuel, 1995; Bister and Emanuel, 1998; Bryan and Rotunno, 2009).

The issues relating to the boundary-layer formulation, the far-field outflow layer and sources of relative angular momentum discussed above were not considered in the recent textbook articulation of Emanuel's steady-state hurricane model by Holton and Hakim (2012).

### 6.2. *Wirth and Dunkerton's model*

Wirth and Dunkerton (2006, henceforth WD06) describe a model that purports ' ... to provide a unified perspective on the dynamics of hurricane- and monsoon-like vortices by identifying them as specific limiting cases of a more general flow system'. This more general system consists of a stationary axisymmetric flow of a stably stratified non-Boussinesq atmosphere in gradient wind balanced on an $f$-plane. The flow is forced by a pattern of heating or cooling by relaxing the temperature to a specified equilibrium temperature, $T_e$, in analogy to the model for the Hadley circulation of Schneider (1977) and Held and Hou (1980). The model is nearly inviscid in the flow interior and is bounded by a rigid wall and rigid upper lid. The flow is attenuated by surface friction that is represented implicitly through an Ekman-like boundary condition relating the vertical velocity at the lowest model level to the vertical component of relative vorticity there. Elsewhere, the flow is assumed to be almost inviscid. The heating and cooling is such that it gives rise to an overturning circulation. Numerical solutions are obtained by time-stepping the thermodynamic equation to a steady state, where at each step the Eliassen secondary circulation is diagnosed.

Cyclonic *RAM* is exchanged primarily at the lower boundary. In all cases, the upper anticyclone associated with the vortex descends to the surface. Cyclonic *RAM* is lost in the core region where the flow is cyclonic and it is replenished in the outer region beyond a certain radius where the flow is anticyclonic. Unlike the E86 model, no significant sources of cyclonic angular momentum are supplied at the outer radius or the upper troposphere. In this forced model, a steady-state solution is achieved, the structure of which depends, *inter alia*, on the relaxation rate.

The numerical simulation presented in section 3 has some aspects in common with this solution, but, as the anticyclone descends, the integrated *RAM* rapidly decreases and the vortex weakens. At the same time, the convective forcing in the core region weakens markedly (not shown). A major difference is that the anticyclone does not descend all the way to the surface. WD06 note that ' ... global constraints from angular momentum conservation are observed to a satisfying degree', but they do not

discuss the individual sources and sinks of angular momentum in their model. However, if WD06's steady state is a global one, it can be inferred that the cyclonic angular momentum lost by surface friction in the inner region must also be replenished at the surface. This replenishment occurs at large radii, where the flow is anticyclonic.

### 6.3. *Hakim's model*

We now examine the statistical equilibrium solutions of Hakim (2011), based on an axisymmetric model. Hakim's study appears to be motivated in part by the fact that 'most earlier studies used a damping scheme on the temperature field as a parametrization of radiative cooling, which the authors (*sic*) demonstrate yields storms that have little convection outside the eyewall and do not achieve statistical equilibrium'. It is true that, as an upper-level warm core develops and expands radially, local convective instability outside the eyewall region would tend to decline, unless there are processes to replenish the instability. These processes would include radiative cooling and/or locally enhanced surface moisture fluxes brought about by a radial expansion of the tangential wind field. Certainly, on time-scales of a few days, a stabilization as a storm matures would appear to be quite realistic and is consistent with experience from aircraft reconnaissance observations.

Traditionally, the expedient of using a Newtonian relaxation scheme has been chosen to avoid an excessive stabilization over integration times of many days and possible changes in the ambient sounding as warm air is advected through the open boundary of the flow domain at large radius. Indeed, the expedient recognizes that the vertical thermal structure of the surrounding tropical atmosphere is, to a first approximation, in a state of radiative–convective equilibrium that is determined by processes occurring on a much larger scale than the tropical cyclone itself.

For the foregoing reasons, in their idealized tropical cyclone simulations, Rotunno and Emanuel (1987) first constructed ambient temperature and moisture profiles that were convectively neutral to their model physics by integrating the model for a sufficiently long period of time without a vortex. Then, in their vortex simulations, they relaxed the temperature profile to the convectively neutral profile. In our view, this procedure is certainly adequate for integrations on forecast time-scales in a given environment, but it is unclear to us that it would become less adequate on longer time-scales, at least as a basis for obtaining theoretical insight of the mature storm and its possible demise.

Hakim presented a calculation with a temperature relaxation scheme similar to the one described herein, but using an axisymmetric model. Surprisingly to us, because the vortex decays, Hakim considers the temperature relaxation scheme to be a flaw of the traditional formulation. When he replaced this scheme by a sophisticated radiative cooling scheme, he was able to simulate a vortex with a quasi-steady maximum intensity of 66 m s$^{-1}$ for approximately 400 days, even in the absence of an initial vortex! It turns out that, as in the illustrative calculation presented herein, Hakim applies a damping layer to momentum and potential temperature within 5 km of the model top (25 km high) and to momentum within 100 km of the outermost radius. This radius is typically 1500 km in both simulations, irrespective of the radiation scheme.

The momentum damping layer in the upper troposphere/lower stratosphere is applied to damp the reflection of vertically propagating gravity waves, but it acts also to restore the flow towards a resting state, thereby acting as a source of cyclonic angular momentum. The damping layer applied near the outer radius plays a similar role to the supply of cyclonic relative angular momentum in the E86 model discussed above. Inspection of Hakim's figure 2 suggests that it is near the outer boundary where much of the cyclonic angular momentum is restored, typically between heights of 5 and 7 km, where air parcels cross a large gradient in the $M$ surfaces as they descend in that region. One might question the physical process in the atmosphere that this restoration scheme represents on a time-scale of 500 days but, given the dramatic differences in vortex evolution between his two simulations, one with a relaxation scheme and the other with a radiative cooling scheme, a further question remains as to how the radiative cooling scheme can have such a large impact on the supply of cyclonic angular momentum to the system to prevent its ultimate demise.

### 6.4. *Bryan's model*

Bryan (2012) criticized the methodology used in a recent study of the sensitivity of tropical cyclone intensification by Montgomery *et al.* (2010), arguing that the solutions presented had not been integrated for long enough to achieve an approximately steady state. Bryan (*op. cit.*, p. 1957) stated that "Using a different primitive-equation model, Bryan and Rotunno (2009) integrated numerical solutions for 12 days in order to achieve an approximately steady state", the implication being that if one integrates for long enough, an approximate steady state will be achieved. Here, 'steady state' refers to the behaviour of the azimuthally averaged tangential wind maximum, which after a period of rapid increase reaches a quasi-steady value. First, we note that the time at which this 'quasi steady state' is achieved will depend on a number of factors including the sea-surface temperature, the ambient thermodynamic sounding, the intensity of the initial vortex and the latitude (Rappin *et al.*, 2011; Smith *et al.*, 2011). However, as intimated in the Introduction, we consider the azimuthally averaged tangential wind maximum to be an insufficient metric by which to adjudicate global steadiness, since the outer cyclonic circulation and upper-tropospheric outflow are often still evolving after the tangential wind maximum has become quasi-steady.

The calculation presented in section 4 used the same model as Bryan and Rotunno (2009), but in a three-dimensional configuration, and reached a quasi-steady state only briefly (the mature stage identified in Figure 2) before decaying steadily. A similar calculation, using an axisymmetric configuration of the model, was run for 30 days. The vortex in this calculation did achieve a quasi-steady intensity between 5 and 8 days, but the intensity declined afterwards, slowly to 16 days and more rapidly thereafter. By 20 days the intensity had reduced to less than 50% of the maximum intensity. As discussed above, the lack of an adequate supply of angular momentum to the system would provide an explanation for the ultimate decay, as in the three-dimensional calculation.

## 7. Conclusions

This study was motivated by several questions that have arisen in our own work and that of several others surrounding the concept of the mature stage of a tropical cyclone vortex. The definition of the mature stage is commonly based on the time period in which the maximum tangential wind is approximately constant. However, in many of our own calculations the outer circulation is by no means steady during this period. In some cases, the storm continues to expand in size even when the maximum tangential wind is approximately constant with time; in other cases, the storm has already begun to contract. In a few extended range calculations that we have carried out, the vortex intensity decreases with time after some period of maximum intensity. To focus on these issues, we considered here the idealized problem of an isolated tropical cyclone vortex on an $f$-plane.

A steady state would require that the convective instability via fluxes of moisture at the underlying sea surface and/or radiative cooling of the upper atmosphere be maintained. This instability in the inner-core region and the radiative cooling provide a pattern of net diabatic heating and cooling that forces an overturning circulation, which is along $M$ surfaces. Above the

 

frictional boundary layer, in the upward branch of the secondary circulation, the diabatic heating associated with moist convection must be consistent with the material conservation of $\theta_e$. In the descending branch of the secondary circulation, where radiative cooling is operative, $\theta_e$ is not materially conserved. However, the radiative cooling must balance the adiabatic warming of air parcels exactly as they descend. Above the boundary layer, these conditions are encapsulated by the vanishing of the spin-up function discussed in the main text.

This simple picture assumes that the upward branch of the secondary circulation takes place in the eyewall and that elsewhere there is subsidence that would bring extremely dry air from the upper troposphere to the surface. Another layer of complexity is the existence of rain bands, shallow convection and convection of moderate vertical extent that serve the role of moistening the dry air descending to the boundary layer. On top of the foregoing issues there is the problem that the steady state would require just the necessary fluxes of sensible and latent heat to maintain the thermodynamic cycle.

On the dynamical side of this problem is the requirement that there must be a supply of cyclonic relative angular momentum to replenish that lost by the frictional torque at the surface. This requires either a radial cyclonic eddy angular momentum flux at some large radius and/or the outflow anticyclone descending to the surface, so that cyclonic relative angular momentum can be diffused into the bulk vortex. As with the foregoing thermodynamic constraints, these sources of cyclonic angular momentum must balance the frictional loss of cyclonic relative angular momentum exactly. Without a sufficient source of cyclonic relative angular momentum to balance that lost by friction to the ocean, the vortex will ultimately decay to zero by the diffusion of the initial cyclonic angular momentum into the sea!

In summary, we have examined the physical constraints that must be satisfied to allow for a steady-state tropical cyclone in an isolated environment, paying particular attention to the vanishing of the spin-up function above the frictional boundary layer and the global absolute angular momentum budget. We conclude that it is unlikely that all these conditions will be met simultaneously and question whether globally steady-state tropical cyclone solutions have merit. We discussed the implications of these findings for previous studies.

Finally, in the three-dimensional numerical tropical cyclone simulation used to focus the study, we have sought to quantify for the first time the partition between the kinetic energy of the cyclone itself and the upper-level anticyclone that it generates as functions of time, showing that the energy of the anticyclone is not small compared with that of the cyclone.

## Acknowledgements

This article was begun during a visit by the authors to the Regional Forecasting Centre in Darwin, Australia in January 2013. We thank the then Acting Director, Todd Smith, and all the staff of the Centre for their warm hospitality during our stay there. We also thank Jim McWilliams for providing some provocative comments on an earlier version of the manuscript. MTM acknowledges the support of NSF Grant AGS-0733380.

## References

Anthes RA. 1974. The dynamics and energetics of mature tropical cyclones. *Rev. Geophys.* **12**: 495–522.

Bister M, Emanuel KA. 1998 Dissipative heating and hurricane intensity. *Meteor. Atmos. Phys.* **65**: 233–240.

Bryan GH. 2012. Comments on 'Sensitivity of tropical-cyclone models to the surface drag coefficient'. *Q. J. R. Meteorol. Soc.* **139**: 1957–1960.

Bryan GH, Fritsch JM. 2002. A benchmark simulation for moist nonhydrostatic numerical models. *Mon. Weather Rev.* **130**: 2917–2928.

Bryan GH, Rotunno R. 2009a. Evaluation of an analytical model for the maximum intensity of tropical cyclones. *J. Atmos. Sci.* **66**: 3042–3060.

Bryan GH, Rotunno R. 2009b. The maximum intensity of tropical cyclones in axisymmetric numerical simulations. *Mon. Wea. Rev.* **137**: 1770–1789.

Bui HH, Smith RK, Montgomery MT, Peng J. 2009. Balanced and unbalanced aspects of tropical-cyclone intensification. *Q. J. R. Meteorol. Soc.* **135**: 1715–1731.

Carrier GF, Hammond AL, George OD. 1971. A model of the mature hurricane. *J. Fluid Mech.* **47**: 145–170.

Durran DR, Klemp JB. 1983. A compressible model for the simulation of moist mountain waves. *Mon. Weather Rev.* **111**: 2341–2361.

Emanuel KA. 1986. An air–sea interaction theory for tropical cyclones. Part I: Steady state maintenance. *J. Atmos. Sci.* **43**: 585–604.

Emanuel KA. 1988. The maximum intensity of hurricanes. *J. Atmos. Sci.* **45**: 1143–1155.

Emanuel KA. 1995. Sensitivity of tropical cyclones to surface exchange coefficients and a revised steady-state model incorporating eye dynamics. *J. Atmos. Sci.* **52**: 3969–3976.

Emanuel KA. 2003. Tropical cyclones. *Annu. Rev. Earth Planet. Sci.* **31**: 75–104.

Emanuel KA. 2004. Tropical cyclone energetics and structure. In *Atmospheric Turbulence and Mesoscale Meteorology*, Fedorovich E, Rotunno R, Stevens B. (eds.): 280 pp. Cambridge University Press: Cambridge, UK.

Gill AE. 1980. Some simple solutions for heat-induced tropical circulation. *Q. J. R. Meteorol. Soc.* **106**: 337–462.

Hakim GJ. 2011. The mean state of axisymmetric hurricanes in statistical equilibrium. *J. Atmos. Sci.* **68**: 1364–1376.

Held IM, Hou AY. 1980. Nonlinear axially symmetric circulations in a nearly inviscid atmosphere. *J. Atmos. Sci.* **37**: 515–533.

Holton JR, Hakim G. 2012. *An Introduction to Dynamic Meteorology* (5th edn). Academic Press: London.

Marks FD, Black PG, Montgomery MT, Burpee RW. 2008. Structure of the eye and eyewall of Hurricane *Hugo* (1989). *Mon. Weather Rev.* **136**: 1237–1259.

Montgomery MT, Smith RK. 2014. Paradigms for tropical-cyclone intensification. *Aust. Meteorol. Oceanogr. J.* (In Press).

Montgomery MT, Smith RK, Nguyen SV. 2010. Sensitivity of tropical cyclone models to the surface exchange coefficients. *Q. J. R. Meteorol. Soc.* **136**: 1945–1953.

Montgomery MT, Davis C, Dunkerton T, Wang Z, Velden C, Torn R, Majumdar S, Zhang F, Smith RK, Bosart L, Bell MM, Haase JS, Heymsfield A, Jensen J, Campos T, Boothe MA. 2012. The Pre-Depression Investigation of Cloud Systems in the Tropics (PREDICT) experiment: Scientific basis, new analysis tools, and some first results. *Bull. Am. Meteorol. Soc.* **93**: 153–172.

Nguyen SV, Smith RK, Montgomery MT. 2008. Tropical-cyclone intensification and predictability in three dimensions. *Q. J. R. Meteorol. Soc.* **134**: 563–582.

Nicholls ME, Montgomery MT. 2013. An examination of two pathways to tropical cyclogenesis occurring in idealized simulations with a cloud-resolving numerical model. *Atmos. Chem. Phys.* **13**: 5999–6022.

Ooyama KV. 1969. Numerical simulation of the life cycle of tropical cyclones. *J. Atmos. Sci.* **26**: 3–40.

Persing J, Montgomery MT. 2005. Is environmental CAPE important in the determination of maximum possible hurricane intensity? *J. Atmos. Sci.* **62**: 542–550.

Persing J, Montgomery MT, McWilliams J, Smith RK. 2013. Asymmetric and axisymmetric dynamics of tropical cyclones. *Atmos. Chem. Phys.* **13**: 12299–12341.

Rappin ED, Morgan MC, Tripoli GJ. 2011. The impact of the outflow environment on tropical cyclone intensification and structure. *J. Atmos. Sci.* **68**: 177–194.

Rotunno R, Bryan GH. 2012. Effects of parameterized diffusion on simulated hurricanes. *J. Atmos. Sci.* **69**: 2284–2299.

Rotunno R, Emanuel KA. 1987. An air–sea interaction theory for tropical cyclones. Part II: Evolutionary study using a nonhydrostatic axisymmetric numerical model. *J. Atmos. Sci.* **44**: 542–561.

Schneider EK. 1977. Axially symmetric steady-state models of the basic state for instability and climate studies. Part II. Nonlinear calculations. *J. Atmos. Sci.* **34**: 280–296.

Shapiro LJ, Montgomery MT. 1993. A three-dimensional balance theory for rapidly-rotating vortices. *J. Atmos. Sci.* **50**: 3322–3335.

Shapiro LJ, Willoughby H. 1982. The response of balanced hurricanes to local sources of heat and momentum. *J. Atmos. Sci.* **39**: 378–394.

Smith RK, Montgomery MT. 2010. Hurricane boundary-layer theory. *Q. J. R. Meteorol. Soc.* **136**: 1665–1670.

Smith RK, Schmidt CW. 2011. An investigation of rotational influences on tropical-cyclone size and intensity. *Q. J. R. Meteorol. Soc.* **137**: 1841–1855.

Smith RK, Montgomery MT, Vogl S. 2008. A critique of Emanuel's hurricane model and potential intensity theory. *Q. J. R. Meteorol. Soc.* **134**: 551–561.

Smith RK, Montgomery MT, Nguyen SV. 2009. Tropical cyclone spin up revisited. *Q. J. R. Meteorol. Soc.* **135**: 1321–1335.

Smith RK, Montgomery MT, Thomsen GL. 2013. Sensitivity of tropical cyclone models to the surface drag coefficient in different boundary-layer schemes. *Q. J. R. Meteorol. Soc.*, doi: 10.1002/qj.2057.

Vigh JL, Schubert WH. 2009. Rapid development of the tropical cyclone warm core. *J. Atmos. Sci.* **66**: 3335–3350.

Wirth V, Dunkerton TJ. 2006. A unified perspective on the dynamics of axisymmetric hurricanes and monsoons. *J. Atmos. Sci.* **63**: 2529–2547.

 